

Journal of Materials Chemistry A

Accepted Manuscript



This article can be cited before page numbers have been issued, to do this please use: V. Barbera, L. Brambilla, A. Porta, R. M. Bongiovanni, A. Vitale, G. Torrisi and M. Galimberti, *J. Mater. Chem. A*, 2018, DOI: 10.1039/C8TA01606B.



This is an Accepted Manuscript, which has been through the Royal Society of Chemistry peer review process and has been accepted for publication.

Accepted Manuscripts are published online shortly after acceptance, before technical editing, formatting and proof reading. Using this free service, authors can make their results available to the community, in citable form, before we publish the edited article. We will replace this Accepted Manuscript with the edited and formatted Advance Article as soon as it is available.

You can find more information about Accepted Manuscripts in the [author guidelines](#).

Please note that technical editing may introduce minor changes to the text and/or graphics, which may alter content. The journal's standard [Terms & Conditions](#) and the ethical guidelines, outlined in our [author and reviewer resource centre](#), still apply. In no event shall the Royal Society of Chemistry be held responsible for any errors or omissions in this Accepted Manuscript or any consequences arising from the use of any information it contains.

1 **Selective edge functionalization of graphene layers with oxygenated groups by means of**
2 **Reimer-Tiemann and domino Reimer-Tiemann / Cannizzaro reactions**

3
4 Vincenzina Barbera^{1*}, Luigi Brambilla¹, Alessandro Porta¹, Roberta Bongiovanni², Alessandra
5 Vitale², Giulio Torrasi¹, Maurizio Galimberti^{1*}

6
7 ¹Politecnico di Milano, Department of Chemistry, Materials and Chemical Engineering “G. Natta”,
8 Via Mancinelli 7, 20131 Milano, Italy

9 ²Politecnico di Torino, Department of Applied Science and Technology, Corso Duca degli Abruzzi
10 24, 10129 Torino, Italy

11
12 **Abstract**

13 Graphene layers were selectively edge-functionalized with oxygenated functional groups,
14 maintaining their bulk structure essentially unaltered. A reaction was performed between
15 polyhydroxylated graphene layers (G-OH) and CHCl₃/KOH/H₂O. When the reaction with
16 KOH/H₂O was performed at 0°C, by adding successive portions of CHCl₃, the functionalization
17 occurred with aldehydic functional groups. When G-OH reacted with CHCl₃/KOH at room
18 temperature, benzylic alcohol and carboxy groups were introduced. XPS, IR, Raman, WAXD
19 analyses indicated that the graphene layers were chemically modified with the abovementioned
20 functional groups, without intercalated and/or absorbed molecules. It can be thus assumed that
21 functionalization of G-OH with aldehydic groups occurred through Reimer-Tiemann reaction and
22 that domino Reimer-Tiemann / Cannizzaro reaction led to aldehyde disproportion. As a further
23 evidence and a first viable usage of the functionalization with aldehydic functional groups, chitosan
24 was crosslinked with the graphene layers, obtaining flexible and electrically conductive carbon
25 papers.

26
27
28
29
30 *Corresponding author. E-mail: vincenzina.barbera@polimi.it (Vincenzina Barbera)

31 *Corresponding author. E-mail: maurizio.galimberti@polimi.it (Maurizio Galimberti)

32
33

34 1. Introduction

35 Graphene [1-3] has indeed exceptional properties: it features high charge-carrier mobilities [4,5], its
36 in-plane thermal conductivity is among the highest for known materials [6], the theoretical elastic
37 modulus is over 1 TPa and the Young modulus is about 1060 MPa [7]. Thanks in particular to their
38 electrical properties, graphene and graphene related materials find application for energy storage
39 devices [8-10] and in fuel cells [11].

40 Such outstanding graphene properties are essentially due to its six atoms aromatic ring core. Any
41 synthesis [7-15] and functionalization [7, 16-22] has therefore the objective to obtain and preserve
42 such structure. In particular, the control of size, shape, and edge structure of graphene layers is a
43 challenging task.

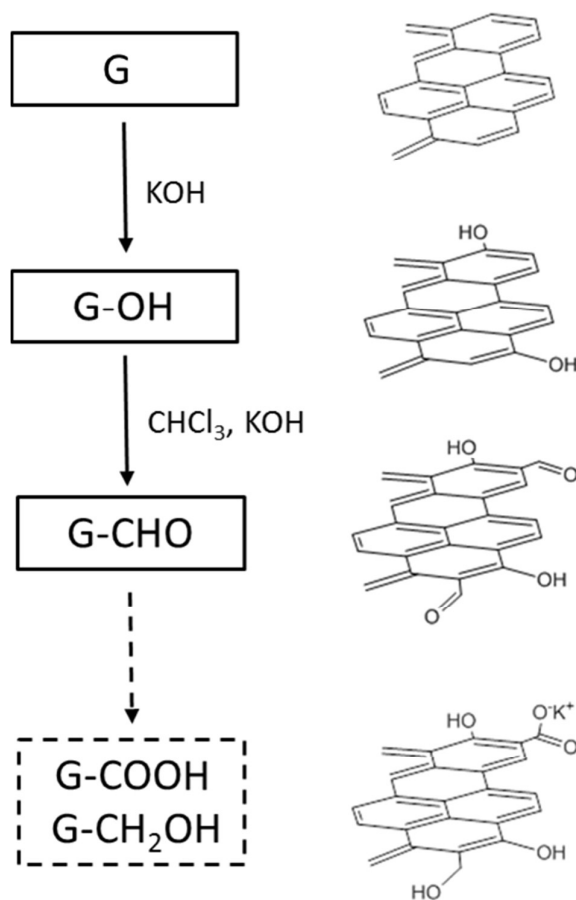
44 Graphene functionalization has great importance. Functional groups affect electronic and solubility
45 properties, self-assembly and phase forming behaviour and can promote further reactions. Over the
46 last years, research has been focused on edge functionalization [3-21], so as to preserve the ideal
47 structure of the graphene core. Edge functionalization has been reported with halogen atoms,
48 [20,21,23-26] converted to nitrile [27] or arylthio [28] groups and used for various metal-catalyzed
49 coupling reactions [29]. Iridium-catalysed direct borylation reaction [30], direct palladium-
50 catalyzed C–H arylation [31] and double C–H activation [32], initializing the construction of novel
51 aromatic structures [33], have also been reported.

52 Great interest is shown for graphene layers with oxygenated functional groups. The chemistry of
53 carboxylic acids has been much explored in the case of carbon nanotubes (CNT) [34]: amidation
54 and esterification reactions have been applied in order to achieve solubility in different solvents, to
55 perform the so-called grafting from polymerizations, to prepare biocompatible sensors. Moreover,
56 graphene and oxygenated derivatives, such as graphene oxide (GO), are being increasingly applied
57 in the field of catalysis [35]. The chemical or thermal reduction of graphene oxide is considered the
58 best practice for large-scale production of graphene [14].

59 However, the introduction of carboxylic groups on CNT and, in particular, the preparation of GO
60 require strong acidic, harsh and even dangerous oxidative conditions [36-46]. The structure of GO
61 has been investigated for decades, but it is still substantially unknown [7,13]. It has been reported
62 [47] that carbonyl and carboxylic groups are on the edges and hydroxy and epoxy groups are on
63 basal planes. Hence, the chemistry that leads to GO cannot be used for the selective edge
64 functionalization of graphene layers. Alternatively, Friedel–Crafts acylation reaction with 4-
65 aminobenzoic acid was performed: it is a one-pot reaction, but requires acidic substances, which
66 could hardly be removed from a graphitic substrate. Another approach reported in the literature for
67 the edge carboxylation is ball milling with carbon dioxide [48]: this method is environmentally

68 friendly, but does not appear ideal for large-scale development. This work describes a new
69 procedure for the edge functionalization of graphene layers with oxygenated functional groups, in
70 particular aldehydes and carboxylic acids or their ester derivatives. It is worth clarifying that
71 reactions were designed to occur on peripheral positions of graphene layers, independently of their
72 organization as single layers or as stacks of few or many layers. Nanosized high surface area
73 graphite (G) with high shape anisotropy (i.e. with a high ratio between the size of crystallites
74 parallel and perpendicular to the structural layers [49]) was chosen as starting material and the
75 synthetic strategy shown in Figure 1 was adopted.

76



77

78 **Figure 1.** Synthetic strategy for the introduction of oxygenated functional groups on the edges of
79 graphene layers G.

80

81 As reported in previous works [50,51], G can be easily functionalised with hydroxyl groups in
82 peripheral position and polyhydroxylated graphene layers are obtained, with substantially unaltered
83 bulk structure. G-OH layers can be considered as a polycyclic aromatic compound, suitable for
84 reactions able to introduce oxygenated functional groups on phenolic substrates. Besides Friedel-
85 Crafts acylation, Reimer-Tiemann reaction [52,53] has been known for a long time as an efficient

86 tool for the preparation of 2-hydroxyaryl aldehydes [52], and is used on an industrial scale for the
87 preparation of salicylic aldehyde (2-hydroxybenzaldehyde), an important intermediate in the
88 chemical industry for the production of fragrances, perfumes, dyes and pharmaceuticals. Studies on
89 Reimer-Tiemann reaction [54] have demonstrated that dichlorocarbene, formed by mixing
90 chloroform with KOH, interacts with the potassium salt of the phenolic substrate in the aqueous
91 phase. By using the same reaction mixture, CHCl_3 in alkaline medium, in the presence of a phase
92 transfer catalyst, cyclopropanation reaction occurs on alkenylic substrates [55] and at the edges of
93 graphene layers [56]. These reagents are not the preferred ones, as cyclopropanes are traditionally
94 formed by adding the methylene–zinc–iodide complex, generated from diethyl zinc and
95 diiodomethane [57-59], or by transition metal-catalyzed decomposition of diazo compounds [60].
96 As G-OH forms stable water dispersions [51] it could thus be a suitable substrate and graphene
97 layers bearing 2-hydroxy aldehyde as functional group should be obtained. However, the selectivity
98 of the Reimer-Tiemann reaction on G-OH cannot be taken for granted. Indeed, it is well known that
99 a strong base, such as KOH, can induce disproportionation of aromatic aldehydes lacking a
100 hydrogen atom in the α -position, promoting the Cannizzaro reaction and leading to benzyl alcohol
101 and potassium benzoate. However, to obtain disproportionation of aldehyde with vanillin as
102 substrate, a catalyst had to be used [61,62] and electrocatalytic effects have been reported to
103 enhance the efficiency of the Cannizzaro reaction [63]. It has to be taken into account that carbon
104 nanostructured materials such as carbon fibers and carbon nanotubes have been used as catalysts for
105 phenol oxidation [64]. Hence, the occurring of Cannizzaro reaction, indicated with the dotted line in
106 the block diagram in Figure 1, cannot be ruled out. Moreover, the introduction of aldehydes in other
107 positions of the graphene layers, which are indeed electron rich, could also be hypothesized. Rather
108 than stretching too far inferences not supported by experimental facts, in this work G-OH was
109 subjected to the Reimer-Tiemann reaction, performed under different experimental conditions: at
110 nominal room temperature, reproducing the experimental conditions usually adopted in the prior art,
111 and at 0°C by adding chloroform in three portions, with the aim of preventing the Cannizzaro
112 disproportionation. Mechanisms for the formation of functionalized graphene layers are proposed.
113 Moreover, reaction of chitosan (CS) with graphene layers bearing aldehydic groups was performed
114 to prepare bionanocomposites.

115

116 2. Experimental

117 2.1 Materials and methods

118 Reagents and solvents were commercially available and were used without further purification:
119 KOH pellets (Carlo Erba Reagenti), chloroform (Aldrich).

120 High surface area graphite (HSAG) was Synthetic Graphite 8427[®] (Asbury Graphite Mills Inc.).
121 Characterization of HSAG has been reported by some of the authors in previous works [49,
122 51,65,66]. Analyses have been repeated on the sample used for the present work, to confirm the
123 reproducibility of what already published.

124 The Fourier-Transform Infrared (FT-IR) spectra were recorded in transmission mode (128 scan and
125 4 cm⁻¹ resolution) in a diamond anvil cell (DAC) using a ThermoElectron Continuum IR
126 microscope coupled with a FT-IR Nicolet Nexus spectrometer.

127 PHI 5000 VersaProbe instrument (Physical Electronics) was used for survey scan and high
128 resolution X-ray photoelectron spectroscopy (XPS). The powder was dried in oven at 100°C for 24
129 h at atmospheric pressure before analysis and thereafter placed in the XPS pre-chamber overnight,
130 in order to avoid anomalous outgassing during the XPS characterization, performed in UHV
131 condition (10⁻⁸ Pa). A monochromatic Al K-alpha X-ray source (1486.6 eV energy, 15 kV voltage
132 and 1 mA anode current) and a power of 25.2 W were used for analysis. Different pass energy
133 values were employed: 187.85 eV for survey spectra and 23.5 eV for high resolution peaks.
134 Analyses were carried out with a take-off angle of 45° and with a 100 μm diameter X-ray spot size
135 on a square area of 1400×1400 μm², with the aim to have a good average and better statistics of
136 powder behavior. A double beam (electron and argon ion gun) neutralization system, dedicated to
137 reduce the charging effect on samples, was also employed during data acquisition. All binding
138 energies (B.E.) were referenced to the C1s line at 284.8 eV. Spectra were analyzed and peak
139 deconvolution was performed using Multipak 9.6 software.

140 Raman spectra were recorded on powdered samples deposited on a glass slide by using an Horiba
141 Jobin Yvon Labram HR800 dispersive Raman spectrometer equipped with Olympus BX41
142 microscope and a 50X objective. The excitation line at 632.8 nm of a He/Ne laser was kept at 0.5
143 mW in order to prevent samples degradation. The spectra were obtained as the average of four
144 acquisitions (30 seconds each) with a spectral resolution of 2 cm⁻¹. The Raman spectra reported in
145 this work are the average of spectra recorded in five different points of the samples.

146 Wide-angle X-ray diffraction (WAXD) patterns were obtained in reflection, with an automatic
147 Bruker D8 Advance diffractometer, with nickel filtered Cu-Kα radiation. Patterns were recorded in
148 10° – 100° as the 2θ range, being 2θ the peak diffraction angle. Distance between crystallographic
149 planes was calculated from the Bragg law. The D_{hkl} correlation length, in the direction

150 perpendicular to the hkl crystal graphitic planes, was determined applying the Scherrer equation
151 (equation (1)).

$$152 \quad D_{hkl} = K \lambda / (\beta_{hkl} \cos \theta_{hkl}) \quad (1)$$

153 where: K is the Scherrer constant, λ is the wavelength of the irradiating beam (1.5419 Å, Cu-K α),
154 β_{hkl} is the width at half height, and θ_{hkl} is the diffraction angle. The instrumental broadening, b , was
155 determined by obtaining a WAXD pattern of a standard silicon powder 325 mesh (99%), under the
156 same experimental conditions. The width at half height, $\beta_{hkl} = (B_{hkl} - b)$ was corrected for each
157 observed reflection with $\beta_{hkl} < 1^\circ$ by subtracting the instrumental broadening of the closest silicon
158 reflection from the experimental width at half height, B_{hkl} .

159

160 *2.2 Reimer-Tiemann reaction performed at nominal room temperature (Procedure 1)*

161 In a round bottomed flask equipped with magnetic stirrer and condenser, KOH powder (3.12 g, 55
162 mmol), CHCl₃ (1.12 mL, 14 mmol) and H₂O (0.5 mL) were added in sequence. G-OH (0.500 g),
163 prepared as reported in ref. 51, was added to such mixture after few seconds, to avoid chloroform
164 decomposition by alkaline ions, well known problem in Reimer-Tiemann reaction performed on
165 phenol ring. The mixture was stirred at room temperature, for 12 hours. After this time, solvent was
166 removed at reduced pressure. The solid was reduced in fine grains in a mortar with a pestel,
167 transferred into a Falcon™ tube (15mL) and water (10 mL) was added. The suspension was
168 sonicated for 10 minutes and centrifuged at 4000 rpm for 10 minutes (3 times). 0.7 g of black
169 powder were obtained.

170

171 *2.3 Reimer-Tiemann reaction performed at nominal 0°C (Procedure 2).*

172 The procedure reported in the previous paragraph was adopted also for the reaction performed at
173 0°C, keeping the round bottomed flask in an ice bath. 0.67 g of black powder were obtained.

174

175 *2.4 Reimer-Tiemann reaction performed at nominal 0°C with sequential addition of CHCl₃* 176 *(Procedure 3)*

177 In a round bottomed flask equipped with magnetic stirrer and condenser, KOH powder (3.12 g, 55
178 mmol), G-OH (0.5 g) and H₂O (0.5 mL) were added in sequence. CHCl₃ (1.12 mL, 14 mmol) was
179 added to such mixture after few seconds in three parts (3 x 0.37 mL). The mixture was stirred at
180 0°C for 12 hours. After this time, solvent was removed at reduced pressure. The solid was reduced
181 in fine grains in a mortar with a pestel, transferred into a Falcon™ tube (15mL) and water (10 mL)
182 was added. The suspension was sonicated for 10 minutes and centrifuged at 4000 rpm for 10
183 minutes. This procedure was repeated three times. Byproduct such as KCl was extracted by water.

184 0.50 g of black powder were isolated. The pH was measured to be 14 immediately after the
185 dispersion of KOH in the reaction medium and 13.8 shortly before the work-up.

186

187 *2.5 Preparation of chitosan based nanocomposites*

188 G-CHO (0.4 g) and chitosan (0.4 g) were mixed for 5 minutes in a mortar with the help of a pestle.
189 The mixture was dispersed in water (8 mL) and 4 drops of an aqueous solution of acetic acid 99.7%
190 (0.010 g, 9.9×10^{-3} mol) were added, obtaining a homogenous suspension. Acetic acid was used in
191 such an amount to lead to the protonation of about 7% of chitosan amino groups.

192 The so obtained water suspension was sonicated for 15 minutes. Casting of G-CHO/CS suspension
193 was performed on a glass plate in which an adhesive tape was used to delimit the area. Sheets were
194 formed after water evaporation, at room temperature and at atmospheric pressure (24 hours).

195

196 **3. Results and discussion**

197 *3.1 Preparation and characterization of graphene layers with oxygenated functional groups*

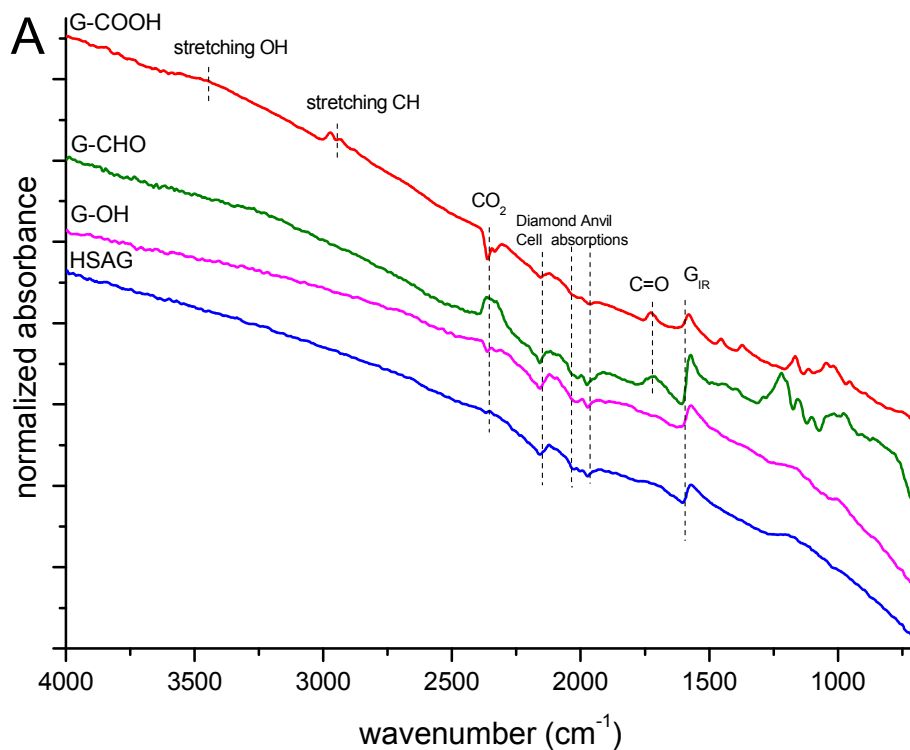
198 Prior to functionalization, the graphitic sample used in this work (HSAG) was duly characterised.
199 Chemical composition, determined by elemental analysis, was (mass %): carbon 99.5, hydrogen
200 0.4, nitrogen 0.1, oxygen 0.0. TGA revealed the following mass loss: 3.2% below 700°C. Surface
201 area was determined by BET according to ASTM D6556 method and was found to be 330.3 m²/g.
202 Average size of HSAG particles was evaluated by means of dynamic light scattering [65], obtaining
203 values representing the hydrodynamic radius of HSAG particles in water dispersions. Average
204 values were 500 nm in the as prepared dispersion and 190 nm after centrifuging the dispersion for
205 30 min centrifugation at 9000 rpm. Transmission electron micrograph taken on supernatant
206 suspension after 60 min centrifugation at 9000 rpm revealed graphite stacks randomly arranged,
207 with lateral size between about 300 nm and 500 nm [51]. FT-IR, XPS and Raman characterization
208 showed that no oxygenated functional group was present prior functionalization (see below).

209 In the first step of the reaction pathway of Figure 1, the high surface area graphite (HSAG) was
210 reacted with KOH, with the help of mechanical energy (through ball milling, details in [51]),
211 obtaining G-OH. Elemental analysis confirmed the results already reported [51]. Elements other
212 than carbon, oxygen, hydrogen and nitrogen were not found. The oxygen content was found to
213 increase to about 6 mass%. A larger mass loss was found for G-OH, below 700° C, than for HSAG.
214 Data are reported in [51]. XPS analysis, commented below in the text, revealed also the presence of
215 potassium. Size of G-OH nanoparticles was evaluated by means of dynamic light scattering and
216 High-Resolution Transmission Electron microscopy (HRTEM). As already reported [51], treatment
217 of HSAG with KOH via ball milling led to the reduction of HSAG aggregates size: from about 190

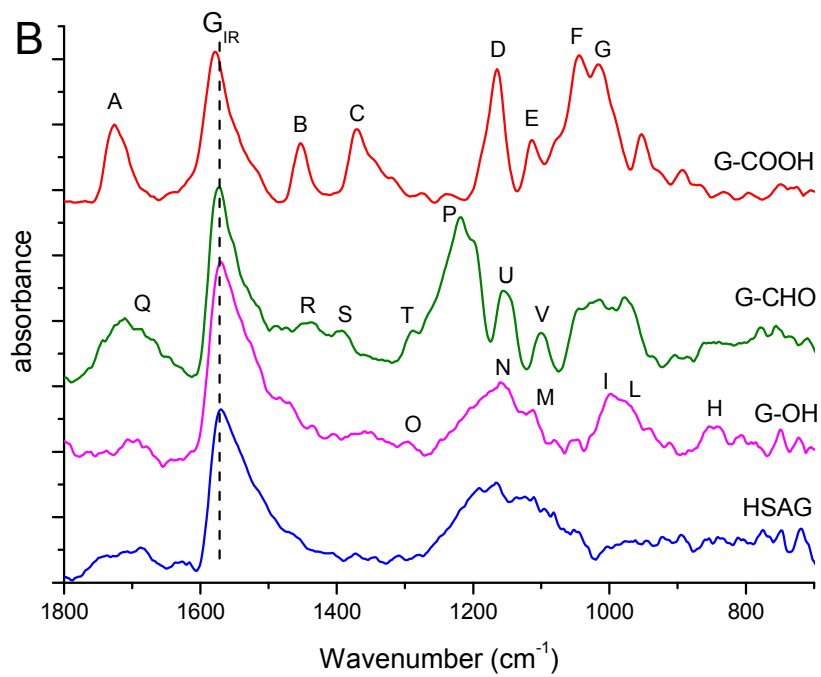
218 nm (HSAG) to about 150 nm, for particles in supernatant suspensions (centrifugation at 9000 rpm
219 for 60 min). TEM micrographs confirmed that the lateral size of HSAG and G-OH were of the same
220 order of magnitude, in samples isolated after centrifugations [51]. These data suggest that the
221 milling step does not cause appreciable breaking of the graphitic layers. Micrographs taken at
222 higher magnification on graphene layers disposed perpendicularly to the beam allowed to visualize
223 stacks with thickness of about 1.7 – 4.8 nm, hence with 6 to 15 stacked graphene layers. Stacks with
224 low number of layers were frequently observed [51].

225 Reaction of G-OH with CHCl_3 was performed by adopting different procedures, described in detail
226 in the experimental part. In a first approach (Procedure 1), KOH powder, CHCl_3 and H_2O were
227 mixed and G-OH was added after few seconds, to avoid chloroform decomposition by alkaline ions,
228 which is known to occur in the case of Reimer-Tiemann reaction performed on phenolic rings. The
229 reaction was performed at 21°C (room temperature in the text) as usually done in the scientific
230 literature [52,53]. An extraordinary reactivity was observed (see Figure S1 in Supplementary
231 Information). To avoid such uncontrolled behaviour, the reaction was carried out at 0°C (Procedure
232 2). Moreover, G-OH, KOH powder and H_2O were mixed at 0°C and CHCl_3 was added in three
233 different steps, in smaller portions (Procedure 3).

234 The characterization of the reactions products was performed by means of IR, XPS, Raman,
235 WAXD spectroscopies. In the following text, products from the reaction carried out at room
236 temperature (Procedure 1) and at 0°C with the successive addition of small CHCl_3 portions
237 (Procedure 3) are described. They are labelled G-COOH and G-CHO, respectively. Product from
238 Procedure 2 is described in the Supplementary Information.



239



240

241 **Figure 2.** FT-IR spectra of HSAG (blue), G-OH (purple), G-CHO (green) and G-COOH (red): in
242 the full region 4000-700 cm^{-1} (A) and zoom in the region 1800-700 cm^{-1} (B). Spectra are displayed
243 after baseline correction.

244

245 In Figure 2A and 2B the IR spectra of the materials under investigation are reported. As explained
246 in detail in the experimental part, IR spectra have been recorded in transmission using a diamond
247 anvil cell (and not in KBr pellet) in order to avoid the presence of the absorption features due to the
248 water molecules that are typically absorbed by KBr during sample preparation. Spectra were
249 obtained from the absorption of very thin films of HSAG particles, which are not transparent to the
250 IR beam. Indeed, the G_{ir} absorption observed in the spectra at 1590 cm^{-1} is mostly due to the
251 reflection from the graphitic planes as revealed by its shape, which resembles a sigmoid function (as
252 expected in specular reflection IR spectroscopy). The strong light diffusion from the HSAG
253 particles is responsible for the increase of the spectra toward high wavenumbers. Details about the
254 interpretation of the signals coming from HSAG and G-OH can be found in previous publications
255 [51,65,66]. Some comments are also reported in this paper to allow direct comparison. The
256 spectrum of the product of the reaction performed at room temperature between CHCl_3/KOH and
257 G-OH (G-COOH) reveals a variety of strong and structured bands, which can be assigned to
258 vibrations of different oxygenated functional groups. It is worth reminding that this family of
259 functional groups show, in IR spectra, the Lorentzian and/or Gaussian profile of an absorption
260 phenomenon. Such profile is observed also in the spectrum of G-CHO in Figure 2. Bands due to G-
261 CHO in Figure 2 appear very different with respect to the signals present in IR spectra of GO or
262 reduced GO. Due to the complexity of the systems, the proposed assignment of the peaks is based
263 on correlative spectroscopy [67]. In Figure 2A the broad and weak absorption at 3400 cm^{-1} can be
264 assigned to -OH stretching vibrations of hydrogen bonded hydroxy groups already present in G-OH.
265 At 1590 cm^{-1} the signal common to all the samples is assigned to the E_{1u} IR active mode of the
266 collective C=C stretching vibration (G_{IR}) of graphitic materials enhanced for the structural
267 disordered and/or chemically functionalization of the graphitic layers. In the spectrum of G-COOH
268 bands at 2967 cm^{-1} , 2928 cm^{-1} and 2874 cm^{-1} (absent both in HSAG and GOH) can be assigned to
269 the CH stretching vibrations of CH_3 and CH_2 units. Therefore they can be associated to the presence
270 of $-\text{CH}_2\text{-OH}$ functional groups (i.e. benzylic alcohol moiety, absent in the spectrum of G-OH).
271 In Figure 2B the spectrum of G-COOH shows a structured band at 1730 cm^{-1} (A) that can be
272 assigned to $-\text{C}=\text{O}$ stretching vibration of $-\text{COOR}$ functionalities (acid and/or ester). The frequency
273 of the stretching of this vibration is compatible with the possible formation of intramolecular
274 hydrogen bonds between $-\text{C}=\text{O}$ and $-\text{OH}$ groups which are close to each other in aromatic

275 compounds such as salicylic acid and its derivatives. The band at 1450 cm^{-1} (B) can be assigned to
276 bending vibrations of CH_2 and CH_3 groups and the broad and asymmetric band at 1371 cm^{-1} (C) to
277 both the CH_3 symmetric bending and the out of plane vibration of $-\text{OH}$ groups. The strong bands at
278 1164 cm^{-1} (D), 1111 cm^{-1} (E), 1042 cm^{-1} (F), and 1014 cm^{-1} (G) can be assigned to the stretching
279 vibrations of C-O-C and C-OH functional groups.

280 In the spectrum of G-OH bands at 846 cm^{-1} (H) and 1000 cm^{-1} (I) can be assigned to vibrations of
281 aryl-OH groups, and bands at 975 cm^{-1} (L), 1121 cm^{-1} (M), 1158 cm^{-1} (N), and 1290 cm^{-1} (O) are
282 compatible with vibration of epoxy or ether groups.

283 The spectrum of G-CHO (i.e. the product of the reaction performed at 0°C with successive
284 additions of small CHCl_3 portions) shows many features observed also for G-OH. A relevant
285 difference is the presence of the strong band at 1220 cm^{-1} (P), and the broad and structured band at
286 1715 cm^{-1} (Q) which can be assigned to $-\text{C}=\text{O}$ stretching vibration of aldehydic functionalities.
287 Other bands at 1438 cm^{-1} (R), 1390 cm^{-1} (S), 1290 cm^{-1} (T), 1158 cm^{-1} (U), and 1100 cm^{-1} (V) have
288 a good correspondence with the absorptions of benzaldehyde and salicylaldehyde [68] molecules.

289 The IR spectroscopic evidences indicate that the reaction between G-OH and CHCl_3/KOH
290 introduces new functional groups onto the graphene layers. The type of functional groups
291 introduced depend on reactions conditions: $-\text{OH}$, $-\text{COOR}$ (acid and/or ester) and $-\text{CH}_2-\text{OH}$ groups
292 were introduced when the reaction was performed at room temperature and reagents were added in
293 one shot. When the reaction was carried out in milder conditions, at 0°C with successive CHCl_3
294 additions, aldehydic groups were selectively formed. This latter procedure (Procedure 3) seems thus
295 to allow the selective occurring of Reimer-Tiemann reaction. Domino reaction made by Reimer-
296 Tiemann followed by Cannizzaro disproportionation appears instead to occur when the high surface
297 area graphite reacts with KOH/CHCl_3 .

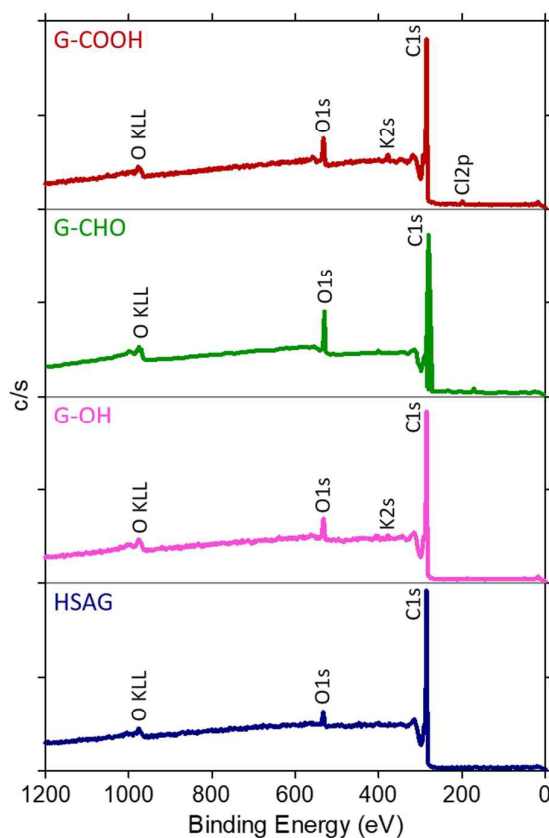
298 XPS spectra of HSAG, G-OH, G-CHO and G-COOH are shown in Figure 3. The main signals of all
299 the samples are due to C_{1s} and O_{1s} . In the case of HSAG, as discussed in [51], a surface oxidation
300 was detected ($\text{O}_{1s}/\text{C}_{1s}=0.04$, 4.2% atomic) while elemental analysis did not reveal the presence of
301 oxygen. G-OH presented however a larger amount of oxygen: $\text{O}_{1s}/\text{C}_{1s}=0.07$, 6.4% atomic.

302 In the XPS wide scan spectrum of G-COOH, besides the two main signals, C_{1s} at B.E.=284.8 eV
303 and O_{1s} at B.E.=533.0 eV, presence of K and Cl is also revealed. The $\text{O}_{1s}/\text{C}_{1s}$ atomic ratio has a
304 value of 0.09, which is higher than the ratio estimated in G-OH (0.07); the oxygen content is 8.2%
305 atomic. The G-CHO sample presents an oxygen content of 10 % atomic and $\text{O}_{1s}/\text{C}_{1s}=0.12$.

306 By the C_{1s} peak deconvolution, three components were detected (see Figure S2 and Table S1 in
307 Supplementary Information). One peak has the same position as that of graphite (284.8 eV), with
308 the characteristic tailing on the high energy side, due to the π bond shake-up satellite, which are

309 clear in the HSAG spectrum [51]. The other two components of C_{1s} are found at higher binding
310 energies, due to the electron withdrawing effect of oxygen. They are attributable to C-O and C=O
311 functions. The C=O/C-O ratio is 0.45 for HSAG, decreases to 0.18 and 0.16 for G-OH and G-
312 COOH respectively. Interestingly the value is 0.55 for G-CHO and this indicates that carbonyl
313 functions are the prevailing ones among the oxidized groups.

314



315

316

Figure 3. Wide scan XPS spectra of HSAG, G-OH, G-CHO and G-COOH.

317

318 To better understand the nature of the oxidized groups, a narrow scan on the O_{1s} peak and its
319 deconvolution was performed (see Figure S3 in Supplementary Information). In fact, analysis of the
320 C_{1s} spectrum does not allow accurate characterization, due to the large contribution of $C\ sp^2$, which
321 tends to mask relative contributions of other groups [69]. Information provided by the analysis of
322 the O_{1s} can therefore better complement the information gathered by the IR spectra. It has however
323 to be taken into account that XPS analysis probes only the outer layer (about 40 Å thick) of the
324 graphitic material and the O_{1s} spectra can be more surface specific than C_{1s} spectra.

325 For G-COOH as for G-OH, there are two main contributions to O_{1s} signal, i.e., at 531.3 eV and
326 533.2 eV, a minor component at 535.2 eV and a negligible signal at 530.4 eV. The main

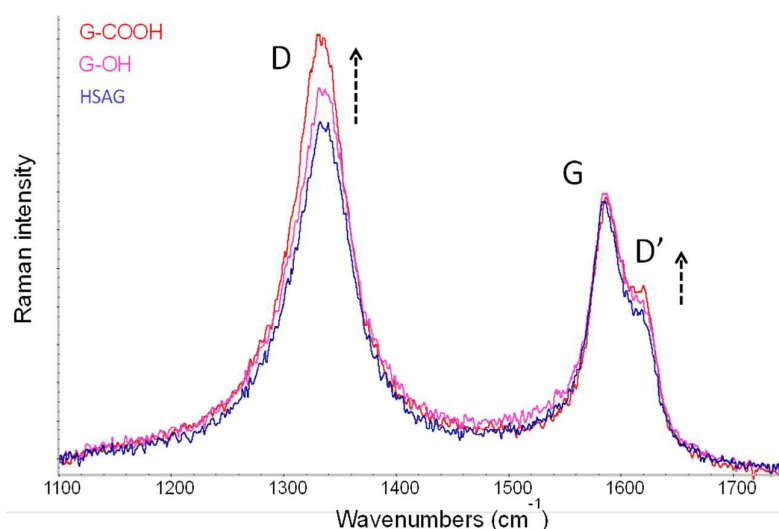
327 components are located at slightly different energies than G-OH. On the basis of the literature data,
 328 one can attribute the signal at 531.3 eV to C=O groups of carbonyl and carboxyl groups (they count
 329 for around 50% of the signal intensity) with a shift of 0.2 eV with respect to G-OH. The component
 330 at 533.2 eV (again 0.3 eV shifted with respect to G-OH) evidences the presence of C-O groups
 331 identified as hydroxyl and ether groups bonded to aromatics. The contribution could account for
 332 both phenolic and benzylic OH, but they cannot be separately identified. The minor component at
 333 higher binding energy can be attributed to adsorbed water and oxygen.

334 In G-CHO, three components appear by deconvoluting the O_{1s} signal: a negligible peak at 530.2 eV
 335 and two main components of similar intensity at 531.5 and 532.9 eV. They could be interpreted as
 336 signals due to C=O groups and C-O groups as in G-COOH. However the second peak appears at a
 337 lower binding energy (532.9 instead of 533.2 eV): it can account for aliphatic C-O but it could also
 338 be a shake-up feature from the C=O peak [70].

339 Both IR and XPS findings indicate the formation of aldehydic derivatives of G-OH, G-CHO, after
 340 the reaction with CHCl₃/KOH at 0°C through Procedure 3. Further oxidized species detected by
 341 XPS appear to be confined in an outer layer. A different product, G-COOH, is obtained, allowing
 342 the occurring of disproportionation Cannizzaro reaction.

343 To demonstrate that the functionalization of the graphene layers does not modify the crystalline
 344 structure, Raman spectroscopy analysis was performed on HSAG, G-OH and G-COOH and spectra
 345 are shown in Figure 4.

346



347
 348 **Figure 4.** Raman spectra of HSAG (red), G-OH (blue) and G-COOH (purple) excited at 632.8 nm.

349

350 All spectra show a similar pattern with the G band at 1582 cm⁻¹ and evident D and D' bands at 1333
 351 cm⁻¹ and 1620 cm⁻¹ respectively. The G peak is assigned to the E_{2g} Raman active mode of collective

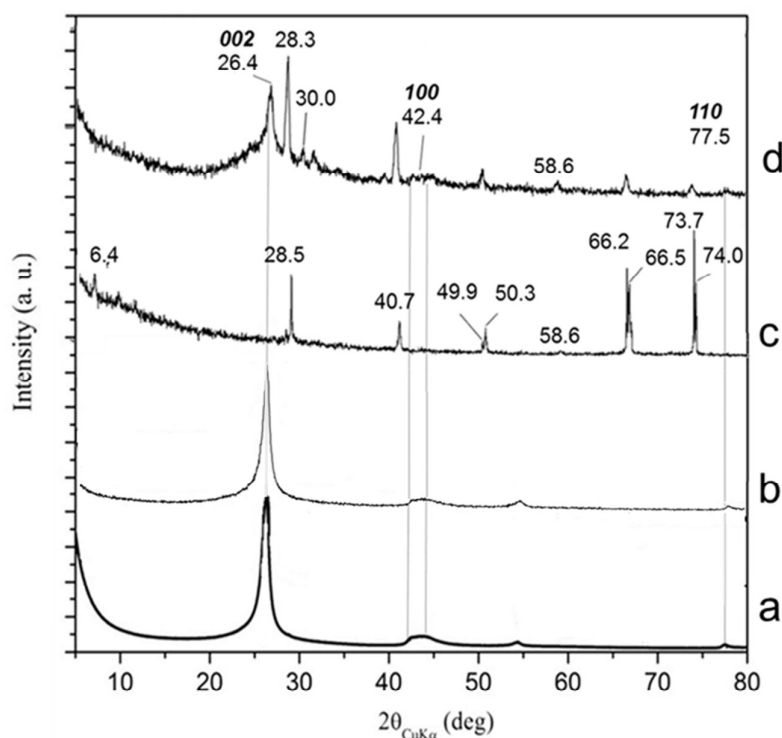
352 C=C stretching vibration of crystalline graphite (graphene), whereas the D and D' peaks appear
353 when structural defects, such as holes, sp^3 or sp carbon atoms, dangling bonds, distortions from
354 planarity, grafted functional groups or confinement (e.g. by edges), affect the graphitic layers. Finite
355 dimensions of the graphitic platelets lead to larger amount of irregular boundaries and, as a
356 consequence, to larger intensity of D and D' peaks [51]. HSAG consists of platelets with a surface
357 of approximately $500 \times 500 \text{ nm}^2$. Such low size can be attributed to the production via ball milling,
358 which cracks the layers, however without substantially altering the in plane order, as revealed by X-
359 ray analysis. The in plane order was maintained also after ball milling with KOH and after the
360 chemical reactions. The enhancement of D band in the spectrum of G-OH can be thus assigned to
361 the hydroxyl functionalization of graphene edges. A further enhancement of D and D' peaks are
362 observed for G-COOH as consequence of the introduction of additional functional groups after
363 reactions of G-OH with CHCl_3/KOH , while indeed new Raman components between G and D
364 peaks, due to disordered sp^3 carbon structures, are not appreciable [71]. One can conclude that the
365 bulk structure of the graphitic layers is essentially unaffected by the functionalization reaction.

366 The essentially unaltered in plane order and interlayer distance allow to assume that
367 functionalization occurred on peripheral positions, reasonably mainly on sites located around the
368 borders of the platelets. This is consistent with the observed stability of the G peak which does not
369 change either the intensity or the frequency. Frequency shifts of the G peak in graphene or the
370 appearance in graphite of a second component at higher Raman shifts are observed for doped
371 graphene, [72-75] and graphite intercalation compounds [72-76].

372 The inspection of Raman spectra leads to exclude the presence of species intercalated between the
373 graphene layers, because their occurrence should generate frequency shifts and/or a second
374 component of the G peak, as normally observed for intercalated Graphite Intercalation Compounds
375 GICs [72-74]. The intercalation of chemical species in between graphene layers is indeed a relevant
376 aspect to be investigated, when graphene layers undergo chemical reactions. Chemical substances
377 could also be absorbed on the carbon material. As discussed in the next paragraph, the presence of
378 absorbed molecule was also investigated and excluded by performing *ad hoc* experiments.

379 The WAXD pattern in Figure 5 reveals that the (002) reflection of G-OH (Figure 5b) and G-COOH
380 after purification (Figure 5d) are at the same 2θ value as in the pristine HSAG sample (Figure 5a).
381 A number of about 22 stacked layers in G-OH (about 35 were in HSAG [51]) was estimated by
382 applying the Scherrer equation. The presence of 100 and 110 reflections, with intensity similar to
383 the one in pristine HSAG, indicates that G-OH and G-COOH remain substantially unaltered: they
384 are thus formed by a low number of stacked graphene layers, the core of which has the ideal
385 graphitic structure. Interestingly, the WAXD profile of G-COOH before purification (Figure 5c) is

386 different: it shows peaks at 28.5 (200), 40.7 (220), 49.9 (222), 58.6 (400), 66.5 (420), 73.7 (422),
 387 which can be attributed to KCl. It can be assumed that KCl promotes the exfoliation of the material.
 388 In fact, the preparation of exfoliated graphite from hydrothermally synthesized graphite-KCl
 389 compounds has been reported [78]. The removal of KCl by the purification procedure (see
 390 experimental part) can restore the stacking of graphene layers. WAXD patterns, in particular the
 391 (002) reflection at the same 2θ value in HSAG and in the functionalized samples, lead to exclude
 392 the presence of intercalated compounds [79].



393
 394 **Figure 5.** WAXD patterns of HSAG (a), G-OH (b), G-COOH before purification (c) and after
 395 purification (d).
 396

397 Experimental findings discussed so far indicate that the reactions proposed in this work (Figure 1)
 398 preserve the bulk structure of graphene layers through all the processes.

399

400 *3.2 Mechanisms proposed for the functionalization reactions of graphene layers*

401 Experimental findings reported above reveal that the reaction of polyhydroxylated graphene layers
 402 with $\text{CHCl}_3/\text{KOH}/\text{H}_2\text{O}$ led to the modification of graphene layers with oxygenated functional
 403 groups.

404 Results from analytical investigations allow to identify the nature of the functional groups:
405 aldehydic groups were observed when the reaction was performed at 0°C and benzyl alcohol and
406 carboxy groups (prevailing ester) when the reaction was carried out at nominal room temperature.
407 Below in the text, it is shown the formation of imines from the reaction of G-CHO with chitosan.
408 This appears a support of the presence of aldehydic groups on the graphene layers.

409 The presence of intercalated oxygenated species can be ruled out on the basis of Raman and WAXD
410 results. As anticipated above, the presence of low molar mass oxygenated molecules only absorbed
411 on the graphene layers was also investigated. G-OH was mixed with an excess of formaldehyde
412 (even though it would be hard to justify the presence of formaldehyde) for 12 hours and FT-IR
413 spectrum was immediately recorded, without observing any modification (The IR spectrum is
414 reported as Supplementary Information S1).

415 In order to elaborate an interpretation of the results so far reported, the scientific literature has to be
416 carefully considered. For example, it was reported that by using the same reaction mixture, CHCl₃
417 in alkaline medium, in the presence of a phase transfer catalyst, cyclopropanation reaction occurs on
418 alkenylic substrates [56] and at the edges of graphene layers [55]. These reagents are not the
419 preferred ones for cyclopropanation, as cyclopropanes are traditionally formed by adding the
420 methylene-zinc-iodide complex, generated from diethyl zinc and diiodomethane [57,58,79], or by
421 transition metal-catalyzed decomposition of diazo compounds [59]. Moreover, cyclopropanation
422 reaction was reported [55] to occur on the graphene layers in the presence of a phase transfer
423 catalyst, which was not used in the work here reported. However, to investigate and, in case, to rule
424 out the formation of cyclopropane ring, pristine HSAG was mixed with KOH powder, CHCl₃ and
425 H₂O. Results of this experiment are reported as Supplementary Information S2. Infrared spectrum is
426 shown in Figure S5. Typical spectral features of cyclopropane rings cannot be detected, confirming
427 that the phase transfer catalyst, as reported in literature [56], is needed.

428 In the light of what discussed so far, the following mechanism can be proposed. The
429 functionalization of graphene layers occurred through Reimer-Tiemann reaction (introduction of
430 aldehydic groups) and domino Reimer-Tiemann / Cannizzaro reaction (benzyl alcohol and carboxy
431 groups). The mechanism for these reactions is presented in Figure S6 and discussed in the following
432 in the Supplementary Information.

433 It is worth summarizing here that the preferred reaction pathway proposes the reaction of the
434 dichlorocarbene, formed by the reaction of KOH with CHCl₃, with the carbon atoms in the ortho
435 positions with respect to the oxygenated group. Only such reactivity, favored by the charge
436 delocalization which increases nucleophilicity of the carbon atoms, can account for the formation of
437 an aldehydic species.

438 The mechanism of the Reimer-Tiemann reaction suggests that oxygenated functional groups are
439 located on the edges of the graphene layers and that a reaction occurs on graphene layers in the
440 armchair configuration, which have two neighboring reactive sites. The Reimer-Tiemann reaction
441 leads to the formation, for each CHO mole, of three KCl moles, which indeed affect the
442 organization of graphene layers, favoring their impressive exfoliation [29], as shown by WAXD
443 results (Figure 5). The functionalization degree of this reaction is reported in the Supplementary
444 Information S3.

445 Figure S6B of the Supplementary Information shows the mechanism for the Cannizzaro
446 disproportionation reaction, which occurs at room temperature and leads to the introduction of
447 benzyl alcohols and carboxy functional groups on graphene layers. Discussion of the mechanism is
448 proposed as well in the Supplementary Information. The Cannizzaro reaction can only occur on
449 aldehydes lacking hydrogen atoms in the α positions. In fact, aromatic substrates with α hydrogens
450 undergo instead deprotonation leading to enolates: these species are not detected in the IR spectra of
451 isolated products. Carboxy functional groups could be due to both acids and esters. The presence of
452 esters could be justified if we hypothesize the condensation of benzyl alcohol and acid groups.
453 Indeed, the Cannizzaro reaction is used on an industrial scale for the preparation of esters starting
454 from aldehydes. In order to estimate to what extent esterification reaction occurred, calculations
455 (reported as Supplementary Information S4) have been attempted. They seem to indicate that
456 esterification reaction may occur. Graphene layers with alcohol and acid functional groups could be
457 then be prepared through hydrolysis.

458 The efficiency of the domino process, documented in Figure S1 (Supplementary Information), can
459 be explained taking into account that both Reimer-Tiemann and Cannizzaro are exothermic
460 reactions, in particular the former one. In spite of such efficiency, the bulk structure of graphene
461 layers was substantially unaltered and this is in line with functionalization on peripheral positions.
462 In the Supplementary Information S5, it is reported the characterization of graphene layers obtained
463 from the reaction of G-OH with KOH/H₂O/CHCl₃ at 0°C (Procedure 2). It is worth summarizing
464 that disproportionation reaction was not prevented: indeed, aldehydes were detected together with
465 carboxylic acids.

466 It is definitely important pondering why G-OH allows the occurring of the domino reaction. Only
467 speculations can be attempted. Two key steps characterize Cannizzaro disproportionation: (i) the
468 formation of the carboxy group with the expulsion of a hydride ion, (ii) the addition of the hydride
469 ion to a second mole of aldehyde. The carboxy group in G-OH could have high stability thanks to
470 the conjugation allowed by an infinite polycyclic aromatic hydrocarbon such as graphene. Such
471 stability allows an easy leaving of the hydride ion, which could be adsorbed on the graphene layer,

472 as potassium salt. Indeed, the absorption on graphene of hydrides of electropositive metals is
473 studied as tool for hydrogen storage [80]. Moreover, it could also be hypothesized that electron rich
474 G-OH adsorbs the reagents, acting as a catalyst for oxidation promoted by the oxygen dissolved in
475 the alkaline medium.

476 According to the reported mechanisms, the functionalization should occur on the edges of the
477 graphene layers. This could account for the difference of the IR spectra of the present work with
478 respect to the IR spectra of GO or reduced GO, where functional groups are expected over the entire
479 graphene plane. Moreover, Cannizzaro disproportionation reaction is known to occur moving from
480 aldehydes in the absence of acidic hydrogen on the alpha carbons, as it would be G-CHO. It is not
481 the purpose of this work to stretch inferences too far. However, a good number of experimental data
482 and analytical indications seem to support the plausibility of the above reported mechanisms. More
483 than that, they indicate that graphene layers were chemically modified with oxygenated functional
484 groups.

485

486 *3.3 Nanocomposites based on G-CHO and chitosan*

487 With the aim to prove a viable use of functionalized graphene layers, exploiting the aldehydic
488 groups, bionanocomposites were prepared based on G-CHO and chitosan. The objective was to
489 crosslink chitosan with the graphene layers, thanks to the reaction between aldehydes and amino
490 groups. It is well known that chitosan can be crosslinked by dialdehydes and a molecule such as
491 glutaraldehyde is traditionally used [81], in spite of its critical aspects as for the impact on human
492 health. In the scientific literature, nanocomposites based on chitosan and graphene related materials
493 (i.e., graphene oxide or reduced graphene oxide) have been reported for different applications, such
494 as the preparation of highly compatible membranes [82], the detection of human epidermal growth
495 [83] and bone tissue engineering [84]. Improved properties are expected for the bionanocomposite
496 based on chitosan and G-CHO, thanks to the unperturbed nature of the graphene layers. To verify
497 the feasibility of the crosslinking reaction of G-CHO with amino groups, hexamethylenediamine
498 was successfully used as the crosslinking agent. Results are reported as Supplementary Information
499 S6. In this manuscript, reaction of G-CHO with chitosan and main materials molecular features are
500 reported, while the assessment of its physico-mechanical properties will be the focus of a future
501 work.

502 Reaction between G-CHO and CS was performed as described in the experimental part and
503 schematically shown in Figure 6.

504

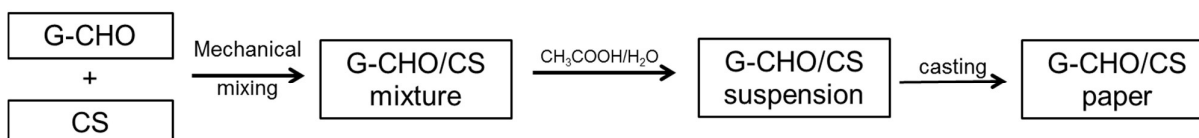


Figure 6. Block diagram for the preparation of G-CHO/CS paper.

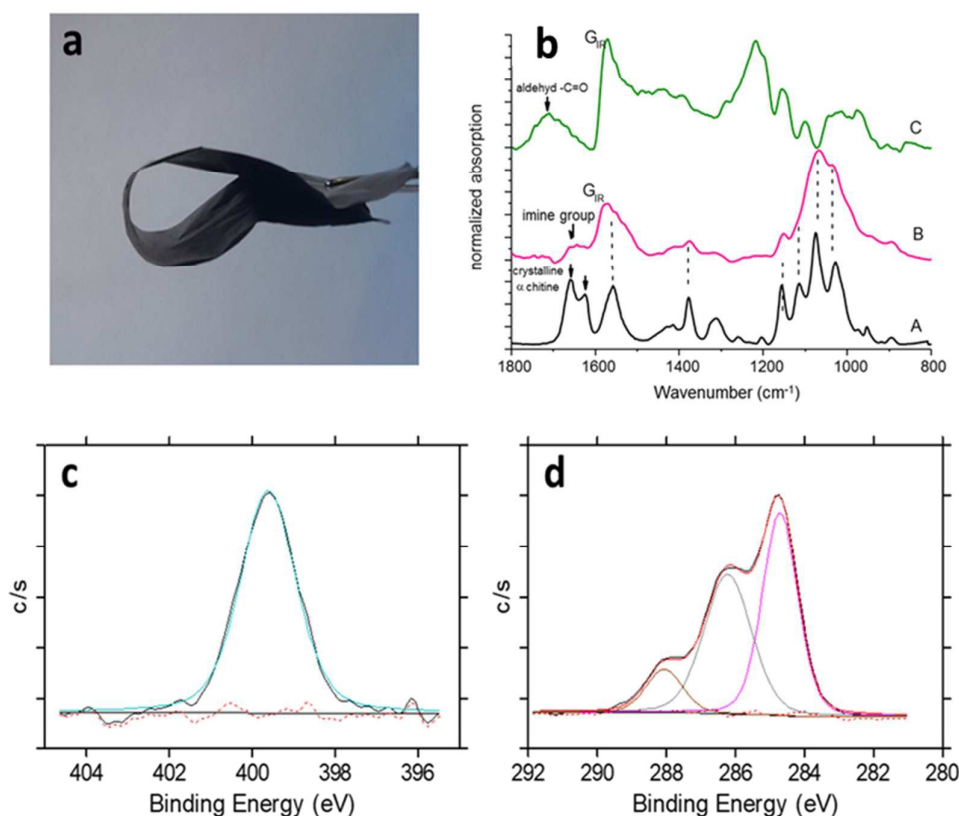
In brief, G-CHO and CS were first premixed in a mortar with the help of a pestle. Water dispersion of the formed adduct was prepared in the presence of acetic acid. These dispersions were stable for at least 1 week. Flexible carbon paper (Figure 7a) was then prepared by simply casting the dispersion on a glass support and waiting for water evaporation. Characterization of G-CHO/CS carbon paper was performed by means of FT-IR (Figure 7b) and XPS (Figure 7c and 7d).

In Figure 7b, spectra of solid CS, G-CHO/CS paper and G-CHO are reported in the region 1800 – 800 cm^{-1} . In the spectrum of pure CS (A) the strong and structured band at 1558 cm^{-1} with a shoulder at 1575 cm^{-1} could be assigned to the overlap of the -CN- stretching (amide II) of the C=ONHCH₃ group (chitin units) and of the -NH₂ bending vibration of the primary amine (deacetylated chitin units). The sharp peak at 1378 cm^{-1} is assigned to the symmetric bending of methyl groups (“umbrella” motion of chitin groups). The four strong and sharp peaks in the region 1200 cm^{-1} - 1000 cm^{-1} could be assigned to CO stretching modes of -COH, -COC- and -CH₂OH groups of the glycosidic ring [85]. The occurrence of sharp and well-defined absorption bands and of the doublet at 1659 cm^{-1} and 1625 cm^{-1} (assigned to NH bending in crystalline α -chitin) suggests the presence in the solid of crystalline domains.

In the spectrum of the G-CHO/CS paper (B) the G_{IR} peak at 1590 cm^{-1} and the main absorption of CS can be observed. However, all the absorption bands are broader; there is a peak shift and band overlapping. This observation supports the occurrence of structural disorder CS moiety in the carbon paper. Interestingly the well-defined band at 1715 cm^{-1} (observed in the spectrum of G-CHO and assigned to -C=O stretching vibration of aldehydic functionalities) is strongly reduced in intensity while a new medium-weak feature at 1656 cm^{-1} appears. Although in this region features due to ammidic functionalities of CS are expected, the contemporary presence of the band at 1656 cm^{-1} associated to the strong -C=O stretching reduction highly support the formation of imine groups between CS and G-CHO.

The wide scan XPS spectrum of G-CHO/CS carbon paper contains signals from C_{1s}, O_{1s} and N_{1s}, as expected; minor amounts of Na, Si and Ca are present. Deconvolution was attempted for carbon and nitrogen signals, although it is difficult to precisely assign the individual contribution of the several groups in both the C_{1s} and N_{1s} peak. The N_{1s} narrow scan signal (Figure 7c) presents one component at 399.6 eV: it can account for amine and amide belonging to chitosan (partially

537 deacetylated), imine, imide, amide groups resulting from a reaction between chitosan and the
 538 oxygen containing groups of the carbon material. Therefore the presence of C-N and C=N groups
 539 due to a covalent attachment of the macromolecule to the functionalized graphene can be predicted.
 540 The deconvolution of the C_{1s} peak results in three components (Figure 7d). The one at 284.7 eV
 541 corresponds to sp^3 carbon and can also be assigned to C-N groups which have been formed by the
 542 already commented direct reaction of the polyamines with the C=C double bonds of the carbon
 543 material. The component at 286.2 eV can be assigned to imine groups (C=N) and C-O. Other
 544 carbon-nitrogen and C=O groups cause the component at 288.1 eV. These data can suggest the
 545 covalent bonding of G-CHO and the amino groups of chitosan, namely the imino groups coming
 546 from the reaction of the carbonyl functions introduced by the Riemer-Tieman functionalization.
 547 Comparing the C_{1s} narrow scan XPS spectra of G-CHO/CS carbon paper to those collected on
 548 chitosan mixed with HSAG [65], binding energy shifts are observed, which can further prove the
 549 covalent linking.



550
 551 **Figure 7.** (a) Image of the flexible G-CHO/CS carbon paper; (b) FT-IR spectra of CS (A), G-
 552 CHO/CS carbon paper (B) and C-CHO (C) in the region 1900-700 cm^{-1} ; (c) and (d) XPS narrow
 553 scans and peak deconvolution of N_{1s} (c) and C_{1s} (d) signals of G-CHO/CS carbon paper.
 554
 555

556 **4. Conclusions**

557 Polyhydroxylated graphene layers reacted with KOH/H₂O and CHCl₃. When the reaction was
558 performed at 0°C and CHCl₃ was added sequentially in small portions, aldehydic groups were
559 detected on the graphene layers, as revealed by FT-IR spectra, XPS analysis and by the formation of
560 imine functional groups after the reaction with the primary amines of chitosan. The presence of
561 aldehydic functional groups can be justified by the occurring of Reimer-Tiemann reaction, which is
562 well known to happen to phenolic substrates reacted with CHCl₃ in alkaline medium. When the
563 reaction was performed at room temperature, benzyl alcohol and carboxy (prevaillingly ester)
564 groups were detected on the graphene layers. The Cannizzaro disproportionation reaction is known to
565 lead to such functional groups moving from aldehydes in the absence of acidic hydrogen on the
566 alpha carbons and could thus occur on the polyhydroxylated graphene layers that underwent
567 Reimer-Tiemann reaction. Therefore it can be assumed that domino Reimer-Tiemann / Cannizzaro
568 reaction occurred.

569 Graphene layers were thus functionalized with oxygenated functional groups. According to the
570 reaction mechanism proposed, functionalization occurred on the edges of the layers.

571 First proof of concept for a viable usage of the produced graphene layers bearing aldehydic groups
572 was the crosslinking of chitosan, with the preparation of stable water dispersions and flexible
573 carbon papers, without using graphene oxide or reduced graphene oxide. Graphene layers act as
574 crosslinker for chitosan and ingredient to give mechanical resistance, electrical and thermal
575 conductivities to the composite material. Future objectives of the research are to characterize and
576 fully exploit such properties.

577

578 **Acknowledgements**

579 Prof. Attilio Citterio (Politecnico di Milano) is acknowledged for useful discussions.
580 Authors gratefully acknowledge Dr Mario Maggio (Università degli Studi di Salerno) for the help
581 with X-ray experiments and Dr. Eugenio Gibertini (Politecnico di Milano) for CVs measurements.
582 Financial support was from Fondazione Silvio Tronchetti Provera.

583

584 **References**

- 585 [1].Novoselov, K. *et al.* Electric field effect in atomically thin carbon films. *Science* **306**,666–
586 669 (2004).
587 [2].Geim, A. K., MacDonald, A. H. Graphene: Exploring Carbon Flatland. *Phys. Today* **60**, 35-
588 42 (2007).

- 589 [3]. Service, R. F. Carbon sheets an atom thick give rise to graphene dreams. *Science*, **324**, 875
590 (2009).
- 591 [4]. Novoselov, K. S., Geim, A. K., Morozov, S. V., Jiang, D., Katsnelson, M. I., Grigorieva, I.
592 V., Dubonos, S. V., Firsov, A. A. Two-dimensional gas of massless Dirac fermions in
593 graphene. *Nature* **438** (7065): 197-200 (2005).
- 594 [5]. Stoller, M. D., Park, S., Zhu, Y., An, J., Ruoff, R. S. Graphene-based ultracapacitors. *Nano*
595 *Lett.* **8**: 3498-3502 (2008).
- 596 [6]. Chen, S., Wu, Q., Mishra, C., Kang, J., Zhang, H., Cho, K., Cai, W., Balandin, A. A., Ruoff,
597 R. S. Thermal conductivity of isotopically modified graphene. *Nat. Mater.* **11**: 203-207
598 (2012).
- 599 [7]. Soldano, C., Mahmood, A., Dujardin, E. Production, properties and potential of graphene.
600 *Carbon* **48**: 2127–2150 (2010).
- 601 [8]. Ambrosi, A., & Pumera, M., Electrochemically exfoliated graphene and graphene oxide for
602 energy storage and electrochemistry applications. *Chemistry-A European Journal*, **22**(1), 153-
603 159 (2016).
- 604 [9]. Chua, C.K., Pumera, M. Facile labelling of graphene oxide for superior capacitive energy
605 storage and fluorescence applications. *Phys. Chem. Chem. Phys.* **18**, 9673-9681 (2016).
- 606 [10]. Pushparaj V. L.; Shaijumon M. M.; Kumar A.; Murugesan S.; Ci L.; Vajtai R; Linhardt R.
607 J.; Nalamasu O.; Ajayan P. M. Flexible energy storage devices based on nanocomposite
608 paper. *Proc Natl Acad Sci USA*, **104**, 34, 13574–7 (2007).
- 609 [11]. Waje, M. M., Wang, X., Li, W., & Yan, Y. Deposition of platinum nanoparticles on organic
610 functionalized carbon nanotubes grown in situ on carbon paper for fuel cells.
611 *Nanotechnology*, **16**(7), S395 (2005).
- 612 [12]. Grennberg, H., Jansson, U. Synthesis of Graphene and Derivatives. *Science and Technology*
613 *of Atomic, Molecular, Condensed Matter & Biological Systems* **2**: 105–127 (2012).
- 614 [13]. Hernandez, Y., Pang, S., Feng, X., Müllen, K. Graphene and Its Synthesis. *Polymer*
615 *Science: A Comprehensive Reference* **8**: 415-438 (2012).
- 616 [14]. Eigler, S., Grimm, S., Hof, F., Hirsch, A. Graphene oxide: a stable carbon framework for
617 functionalization. *J. Mater. Chem. A* **1**: 11559-11562 (2013).
- 618 [15]. Randviir, E. P., Brownson, D. A. C., Banks, C. E. A decade of graphene research:
619 production, applications and outlook. *Mater. Today* **17** (9): 426-432 (2014).
- 620 [16]. Yang, H., Li, F., Shan, C., Han, D., Zhang, Q., Niu, L., Ivaskab, A. Covalent
621 functionalization of chemically converted graphene sheets via silane and its reinforcement. *J.*
622 *Mater. Chem.* **19**: 4632–4638 (2009).

- 623 [17]. Swager, T. M. Functional Graphene: Top-Down Chemistry of the π -Surface. *ACS Macro*
624 *Lett.* **1**: 3–5 (2012).
- 625 [18]. Zaman, I., Kuan, H.-C., Meng, Q., Michelmore, A., Kawashima, N., Pitt, T., Zhang, L.,
626 Gouda, S., Luong, L., Ma, J. A Facile Approach to Chemically Modified Graphene and its
627 Polymer Nanocomposites. *Adv. Funct. Mater.* **22** (13): 2735–2743 (2012).
- 628 [19]. Chua, C. K., Pumera, M. Covalent chemistry on graphene. *Chem. Soc. Rev.* **42**: 3222–3233
629 (2013).
- 630 [20]. Bhattacharjya, D., Jeon, I.Y., Park, H.Y., Panja, T., Beom Baek, J., Yu J.S., Graphene
631 Nanoplatelets with Selectively Functionalized Edges as Electrode Material for
632 Electrochemical Energy Storage. *Langmuir*, **31**, 5676–5683 (2015).
- 633 [21]. Xiong, P., Zhu, J., Zhang, L., Wang, X., Recent advances in graphene-based hybrid
634 nanostructures for electrochemical energy storage. *Nanoscale Horiz.*, **1**, 340–374 (2016).
- 635 [22]. Kausar, A., Anwar, Z., Khan, L. A., Muhammad, B., Functional graphene nanoplatelet
636 reinforced epoxy resin and polystyrene-based block copolymer nanocomposite, *Fullerenes*
637 *nanotubes and carbon nanostructures*, **25**(1), 47–57 (2017).
- 638 [23]. Tan, Y.-Z., Yang, B., Parvez, K., Narita, A., Osella, S., Beljonne, D., Feng, X., Mullen, K.,
639 Atomically precise edge chlorination of nanographenes and its application in graphene
640 nanoribbons, *Nat. Commun.*, **4**, 2646 (2013).
- 641 [24]. Xu, J., Jeon, I.-Y., Seo, J.-M., Dou, S., Dai, L., Baek, J.-B., Edge-Selectively Halogenated
642 Graphene Nanoplatelets (XGnPs, X= Cl, Br, or I) Prepared by Ball-Milling and Used as
643 Anode Materials for Lithium-Ion Batteries. *Adv. Mater.*, **26**, 7317 (2014).
- 644 [25]. Zhan, L., Yang, S., Wang, Y., Wang, Y., Ling, L., Feng, X., Fabrication of Fully
645 Fluorinated Graphene Nanosheets Towards High-Performance Lithium Storage. *Adv. Mater.*
646 *Interfaces*, **1**, 1300149 (2014).
- 647 [26]. Jeon, I.-Y., Ju, M. J., Xu, J., Choi, H.-J., Seo, J.-M., Kim, M.-J., Choi, I. T., Kim, H. M.,
648 Kim, J. C., Lee, J.-J., Liu, H. K., Kim, H. K., Dou, S., Dai L., Baek, J.-B., Edge-Fluorinated
649 Graphene Nanoplatelets as High Performance Electrodes for Dye-Sensitized Solar Cells and
650 Lithium Ion Batteries. *Adv. Funct. Mater.*, **25**, 1170 (2015).
- 651 [27]. Ito, S., Wehmeier, M., Brand, J. D., Kübel, C., Epsch, R., Rabe J. P., Müllen, K., Synthesis
652 and Self-Assembly of Functionalized Hexa-peri-hexabenzocoronenes. *Chem. Eur. J.*, **6**, 4327
653 (2000).
- 654 [28]. Tan, Y.-Z., Osella, S., Liu, Y., Yang, B., Beljonne, D., Feng X., Müllen, K. Sulfur-
655 Annulated Hexa-peri-hexabenzocoronene Decorated with Phenylthio Groups at the Periphery.
656 *Angew. Chem., Int. Ed.*, **54**, 2927 (2015).

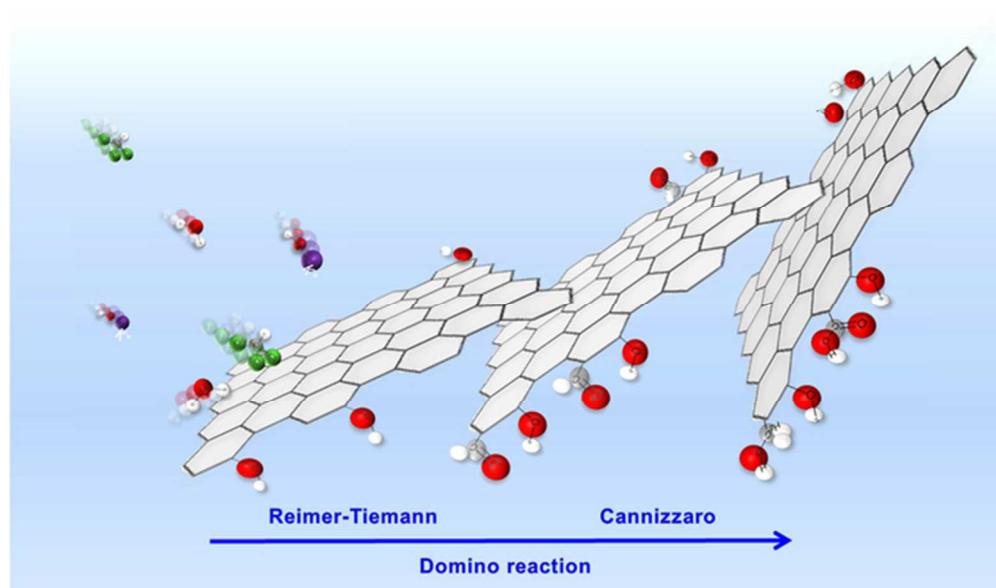
- 657 [29]. Swain, A. K., & Bahadur, D. Facile synthesis of twisted graphene solution from graphite-
658 KCl. *RSC Advances*, **3**(42), 19243-19246 (2013).
- 659 [30]. Mkhaliid, I. A. I., Barnard, J. H., Marder, T. B., Murphy, J. M., Hartwig, J. F., C- H
660 activation for the construction of C- B bonds. *Chem. Rev.*, **110**, 890 (2009).
- 661 [31]. Mochida, K., Kawasumi, K., Segawa Y., Itami, K., Direct arylation of polycyclic aromatic
662 hydrocarbons through palladium catalysis. *J. Am. Chem. Soc.*, **133**, 10716 (2011).
- 663 [32]. Ozaki, K., Kawasumi, K., Shibata, M., Ito H., Itami, K. One-shot K-region-selective
664 annulative π -extension for nanographene synthesis and functionalization. *Nat. Commun.*, **6**,
665 6251 (2015).
- 666 [33]. Kawasumi, K., Zhang, Q., Segawa, Y., Scott L. T., Itami, K. A grossly warped
667 nanographene and the consequences of multiple odd-membered-ring defects. *Nat. Chem.*, **5**,
668 739 (2013).
- 669 [34]. Singh, P., Campidelli, S., Giordani, S., Bonifazi, D., Bianco, A., Prato, M. Organic
670 functionalisation and characterisation of single-walled carbon nanotubes, *Chem. Soc. Rev.*, **38**,
671 2214–2230 (2009).
- 672 [35]. Chua, C. K., Pumera, M. Carbocatalysis: The State of “Metal-Free” Catalysis. *Chem. Eur. J.*
673 **21**: 12550 – 12562 (2015).
- 674 [36]. Brodie, B.C. On the atomic weight of graphite. *Philos. Trans. R. Soc. Lond.* **14**: 249–259
675 (1859).
- 676 [37]. Lopez, M. I., Croce, A. E., Sicre, J. E. Explosive decomposition of gaseous chlorine dioxide.
677 *J. Chem. Soc. Faraday Trans.* **90** (22): 3391–3396 (1994).
- 678 [38]. McAllister, M. J., Li, J.-L., Adamson, D. H., Schniepp, H. C., Abdala, A. A., Liu, J.,
679 Herrera-Alonso, M., Milius, D. L., Car, R., Prud'homme, R. K., Aksay, I. A. Single sheet
680 functionalized graphene by oxidation and thermal expansion of graphite. *Chem. Mater.* **19**
681 (18): 4396–4404 (2007).
- 682 [39]. Staudenmaier, L. Verfahren zur Darstellung der Graphitsäure. *Ber. Dtsch. Chem. Ges.* **31**:
683 1481-1487 (1898).
- 684 [40]. Hummers, W. S., Offeman, R. E. Preparation of Graphitic Oxide. *J. Am. Chem. Soc.* **80**:
685 1339-1339 (1958).
- 686 [41]. Ang, P. K., Wang, S., Bao, Q., Thong, J. T. L., Loh, K. P. High-throughput synthesis of
687 graphene by intercalation–exfoliation of graphite oxide and study of ionic screening in
688 graphene transistor. *ACS Nano* **3** (11): 3587–3594 (2009).
- 689 [42]. Chen, J., Yao, B., Li, C., Shi, G. An improved Hummers method for eco-friendly synthesis
690 of graphene oxide. *Carbon* **64**: 225–229 (2013).

- 691 [43]. Chen, J., Li Y., Huang, L., Li, C., Shi, G. High-yield preparation of graphene oxide from
692 small graphite flakes via an improved Hummers method with a simple purification process.
693 *Carbon* **81**: 826–834 (2015).
- 694 [44]. Guerrero-Contreras, J., Caballero-Briones, F. Graphene oxide powders with different
695 oxidation degree, prepared by synthesis variations of the Hummers method. *Mater. Chem.*
696 *Phys.* **153**: 209-220 (2015).
- 697 [45]. Kovtyukhova, N. I., Ollivier, P. J., Martin, B. R., Mallouk, T. E., Chizhik, S. A., Buzaneva,
698 E. V., Gorchinskiy, A. D. Layer-by-layer assembly of ultrathin composite films from micron-
699 sized graphite oxide sheets and polycations. *Chem. Mater.* **11** (3): 771–778 (1999).
- 700 [46]. Grennberg, H., Jansson, U. Synthesis of Graphene and Derivatives. Science and Technology
701 of Atomic, Molecular, *Condensed Matter & Biological Systems* **2**: 105–127 (2012).
- 702 [47]. Zhu, Y., Murali, S., Cai, W., Li, X., Suk, J. W., Potts, J. R., Ruoff, R. S. Graphene And
703 Graphene Oxide: Synthesis, Properties, And Applications. *Adv. Mater.* **22**: 3906–3924 (2010).
- 704 [48]. Jeon, I. Y., Bae, S. Y., Seo, J. M., & Baek, J. B. Scalable Production of Edge-Functionalized
705 Graphene Nanoplatelets via Mechanochemical Ball-Milling. *Advanced Functional Materials*,
706 **25**(45), 6961-6975 (2015).
- 707 [49]. Mauro, M., Cipolletti, V., Galimberti, M., Longo, P., & Guerra, G. Chemically reduced
708 graphite oxide with improved shape anisotropy. *The Journal of Physical Chemistry C*,
709 **116**(46), 24809-24813 (2012).
- 710 [50]. Yan, L., Lin, M., Zeng, C., Chen, Z., Zhang, S., Zhao, X., & Guo, M. Electroactive and
711 biocompatible hydroxyl-functionalized graphene by ball milling. *Journal of Materials*
712 *Chemistry*, **22**(17), 8367-8371 (2012).
- 713 [51]. Barbera, V., Porta, A., Brambilla, L., Guerra, S., Serafini, A., Valerio, A. M., & Galimberti,
714 M. Polyhydroxylated few layer graphene for the preparation of flexible conductive carbon
715 paper. *RSC Advances*, **6**(90), 87767-87777 (2016).
- 716 [52]. Vibhute, Y. B., Lonkar, S. M., Sayyed, M. A., & Baseer, M. A. Synthesis of substituted 2-
717 hydroxyaryl aldehydes by the microwave-induced Reimer-Tiemann reaction. *Mendeleev*
718 *Communications*, **17**(1), 51 (2007).
- 719 [53]. Crisan, R., & Modra, D. The synthesis of salicylaldehyde varying different parameters.
720 *Annals of West University of Timisoara. Series of Chemistry*, **22**(2), 57 (2013).
- 721 [54]. Hine, J., & Van Der Veen, J. M. The Mechanism of the Reimer-Tiemann Reaction¹. *Journal*
722 *of the American Chemical Society*, **81**(24), 6446-6449 (1959).

- 723 [55]. Corsaro, A., Chiacchio, U., Adamo, R., Pistarà, V., Rescifina, A., Romeo, R., ... & Attolino,
724 E. Steric course of some cyclopropanation reactions of L-threo-hex-4-
725 enopyranosides. *Tetrahedron*, **60**(17), 3787-3795 (2004).
- 726 [56]. Chua, C. K., Ambrosi, A., & Pumera, M. (2012). Introducing dichlorocarbene in
727 graphene. *Chemical Communications*, **48**(43), 5376-5378.
- 728 [57]. Simmons, H. E., & Smith, R. D. (1958). A new synthesis of cyclopropanes from
729 olefins. *Journal of the American Chemical Society*, **80**(19), 5323-5324.
- 730 [58]. Simmons, H. E., Cairns, T. L., Vladuchick, S. A., & Hoiness, C. M. (1973). Cyclopropanes
731 from Unsaturated Compounds, Methylene Iodide, and Zinc-Copper Couple. *Organic*
732 *Reactions*.
- 733 [59]. Pistarà, V., Rescifina, A., Punzo, F., Greco, G., Barbera, V., & Corsaro, A. (2011). Design,
734 Synthesis, Molecular Docking and Crystal Structure Prediction of New Azasugar Analogues
735 of α -Glucosidase Inhibitors. *European Journal of Organic Chemistry*, **36**, 7278-7287 (2011).
- 736 [60]. Sauers, R. R., Schlosberg, S. B., & Pfeffer, P. E. Synthesis and chemistry of some tricyclo
737 [4.2. 1.02, 5] nonane derivatives. *The Journal of Organic Chemistry*, **33**(6), 2175-2181
738 (1968).
- 739 [61]. Pearl, I. A. Reactions Of Vanillin And Its Derived Compounds. Iii. 1 The Cannizzaro
740 Reaction Of Vanillin². *The Journal of organic chemistry*, **12**(1), 79-84 (1947).
- 741 [62]. Pearl, I. A. Silver Catalyzed Reactions Of Phenolic Aldehydes¹. *The Journal of organic*
742 *chemistry*, **12**(1), 85-89 (1947).
- 743 [63]. Rusling, J. F., Segretario, J. P., & Zuman, P. Polarographic reduction of aldehydes and
744 ketones: Part XXIII. Electroreduction of 1-methylpyridiniumcarboxaldehydes. *Journal of*
745 *Electroanalytical Chemistry and Interfacial Electrochemistry*, **143**(1-2), 291-321 (1983).
- 746 [64]. Soria-Sánchez, M., Maroto-Valiente, A., Álvarez-Rodríguez, J., Muñoz-Andrés, V.,
747 Rodríguez-Ramos, I., Guerrero-Ruiza, A., Carbon nanostructured materials as direct catalysts
748 for phenol oxidation in aqueous phase. *Applied Catalysis B: Environmental*, **104**, 101-109
749 (2011).
- 750 [65]. Galimberti, M., Barbera, V., Guerra, S., Conzatti, L., Castiglioni, C., Brambilla, L., &
751 Serafini, A. Biobased Janus molecule for the facile preparation of water solutions of few layer
752 graphene sheets. *RSC Advances*, **5**(99), 81142-81152 (2015).
- 753 [66]. Barbera V., Guerra S., Brambilla L., Maggio M., Serafini A., Conzatti L., ... & Galimberti
754 M., Carbon papers and aerogels based on graphene layers and chitosan: direct preparation
755 from high surface area graphite. *Biomacromolecules*, **18**(12), 3978-3991 (2017).
- 756 [67]. Socrates, G. Infrared Characteristic Group Frequencies, 2nd ed.; Wiley: New York (1980).

- 757 [68]. Boczar, M., Wójcik, M. J., Szczeponek, K., Jamróz, D., Ikeda, S., Theoretical Modeling of
758 Infrared Spectra of Salicylaldehyde and Its Deuterated Derivatives, *International Journal of*
759 *Quantum Chemistry*, **90**, 689–698 (2002)
- 760 [69]. Yang, D., Velamakanni, A., Bozoklu, G., Park, S., Stoller, M., Piner, R. D., ... & Ruoff, R.
761 S. Chemical analysis of graphene oxide films after heat and chemical treatments by X-ray
762 photoelectron and Micro-Raman spectroscopy. *Carbon*, **47**(1), 145-152 (2009).
- 763 [70]. Gustafsson, J. B., Moons, E., Widstrand, S. M., Gurnett, M., & Johansson, L. S. O. Thin
764 PTCDA films on Si (001): 2. Electronic structure. *Surface science*, **572**(1), 32-42 (2004).
- 765 [71]. Ferrari, A. C., Robertson, J., Raman spectroscopy of amorphous, nanostructured, diamond-
766 like carbon, and nanodiamond. *Phil. Trans. R. Soc. Lond. A* **362**, 2477–2512 (2004).
- 767 [72]. Dresselhaus, M. S. Intercalation compounds of graphite, *Advances in Physics*, **51**(1) 1-186
768 (2002).
- 769 [73]. Alsmeyer, D. C. et al. In situ Raman monitoring of electrochemical graphite intercalation
770 and lattice damage in mild aqueous acids. *Anal. Chem.*, **64**, 1528-1533 (1992).
- 771 [74]. Dimiviev, A.M. et al. Reversible formation of ammonium persulfate/sulfuric acid graphite
772 intercalation compounds and their peculiar Raman spectra. *ACS Nano*, **6**(9), 7842–7849
773 (2012).
- 774 [75]. Ferrari, A. C. Raman spectroscopy of graphene and graphite: disorder, electron–phonon
775 coupling, doping and nonadiabatic effects. *Solid state communications*, **143**(1-2) 47-57
776 (2007).
- 777 [76]. Ferrari, A. C. Raman spectroscopy of graphene and graphite: disorder, electron–phonon
778 coupling, doping and nonadiabatic effects. *Solid state communications*, **43**(1-2), 47-57
779 (2007).
- 780 [77]. Zhao, W., Tan, P., Zhang, J., & Liu, J. Charge transfer and optical phonon mixing in few-
781 layer graphene chemically doped with sulfuric acid. *Physical Review B*, **82**(24), 245423
782 (2010).
- 783 [78]. Swain, A. K., & Bahadur, D. Facile synthesis of twisted graphene solution from graphite-
784 KCl. *RSC Advances*, **3**(42), 19243-19246 (2013).
- 785 [79]. Corsaro, A., Chiacchio, M. A., Pistrà, V., Rescifina, A., & Vittorino, E.. Cyclopropanation
786 of 5-methylene galactopyranosides by dihalo-, ethoxycarbonyl-, and unsubstituted carbenes.
787 *Tetrahedron*, **64**(37), 8652-8658 (2008).
- 788 [80]. Tozzini, V., & Pellegrini, V. Prospects for hydrogen storage in graphene. *Physical*
789 *Chemistry Chemical Physics*, **15**(1), 80-89 (2013).

- 790 [81]. Q. Wang; B. Zhang; X. Lin; W. Weng. Hybridization biosensor based on the covalent
791 immobilization of probe DNA on chitosan–multiwalled carbon nanotubes nanocomposite by
792 using glutaraldehyde as an arm linker *Sensors and Actuators B: Chemical* **156**, 599–605
793 (2011).
- 794 [82]. Hung W. S.; Chang S. M.; Lecaros R. L. G.; Ji Y. L.; An Q. F.; Hu C. C.; Lee K. R.; Lai J.
795 Y. Fabrication of hydrothermally reduced graphene oxide/chitosan composite membranes
796 with a lamellar structure on methanol dehydration *Carbon*, **117**, 112-119 (2017).
- 797 [83]. Tabasi A.; Noorbakhsh A.; Sharifi E. Reduced graphene oxide-chitosan-aptamer interface
798 as new platform for ultrasensitive detection of human epidermal growth factor receptor 2.
799 *Biosensors and Bioelectronics* **95**, 117-123 (2017).
- 800 [84]. Peng Yua P.; Bao R. Y.; Shi X. J.; Yang W.; Yanga M.B. Self-assembled high-strength
801 hydroxyapatite / graphene oxide / chitosan composite hydrogel for bone tissue engineering
802 *Carbohydrate Polymers* **155**, 507–515 (2017).
- 803 [85]. Brugnerotto J., Lizardi J., Goycoolea F.M., Argüelles-Monal W., Desbrières J., M.
804 Rinaudo, An infrared investigation in relation with chitin and chitosan characterization
805 *Polymer* **42**, 3569-3580 (2001).
- 806



57x39mm (300 x 300 DPI)